Alternative SiO_2 surface energies direct MCDK epithelial behavior

By: Alan D. Covell, Zheng Zeng, Taylor Mabe, Jianjun Wei, Amy Adamson, and Dennis R. LaJeunesse

A. D. Covell, Z. Zeng, T. Mabe, J. Wei, A. Adamson, D. LaJeunesse, Alternative SiO_2 surface energies direct MCDK epithelial behavior, *ACS Biomaterials Science and Engineering*, **2017**, 3(12) 3307-3317. DOI: 10.1021/acsbiomaterials.7b00645.

Abstract:

The mechanical interactions of cells are mediated through adhesive interactions. In this study, we examined the growth, cellular behavior, and adhesion of MDCK epithelial cells on three different SiO_2 substrates: amorphous glass coverslips and the silicon oxide layers that grow on ⟨111⟩ and ⟨100⟩ wafers. While compositionally all three substrates are almost similar, differences in surface energy result in dramatic differences in epithelial cell morphology, cell–cell adhesion, cell–substrate adhesion, actin organization, and extracellular matrix (ECM) protein expression. We also observe striking differences in ECM protein binding to the various substrates due to the hydrogen bond interactions. Our results demonstrate that MDCK cells have a robust response to differences in substrates that is not obviated by nanotopography or surface composition and that a cell's response may manifest through subtle differences in surface energies of the materials. This work strongly suggests that other properties of a material other than composition and topology should be considered when interpreting and controlling interactions of cells with a substrate, whether it is synthetic or natural.

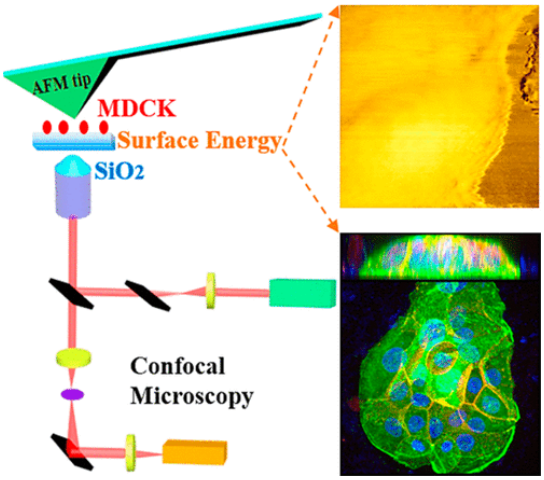

Keywords: MDCK | epithelial morphology | surface energy

Article:

1 Introduction

The response of a cell to any substrate, whether it is natural or synthetic, is governed by the structural and chemical properties of that surface. These properties include the micro- and nanoscale topography of the surface, the presence of specific adhesion molecules on the cell, and the surface material composition.[1-4] Differences in these material properties result in different cellular responses, including alteration to cell morphology, cell fate, and proliferation.[5-9] Many of these responses are linked to cell adhesion mediated mechanical processes regarding both cell–substrate and cell–cell.[8, 10] For the past decade, this fact has been repeatedly demonstrated as cellular interactions with nanostructured surfaces (NSS) guide cell differentiation, control cellular morphogenesis, and can even alter cellular viability.[11, 12] Qualitative differences in the size and shape of the nanoscale features of an NSS determine the nature of the cellular response in subtly different ways.[12] Nanoscale grooves redirect cell polarization and elongation of tissue culture cells in a scale dependent fashion.[13-15] Alteration to the nanoscale structure in the polystyrene polymers of commercial tissue culture plate determines and controls the cell growth rate and viability.[16-18] These studies clearly demonstrate the importance of the nanoscale structure of a substrate on cellular behavior but raise questions regarding the specific nature of influence of nanotopography at the cell/substrate interface.

While a great deal of work has demonstrated the biochemical basis of cell–substrate adhesion, much of these works concentrated on the composition, topology, and mechanical properties of the substrates.[3, 4, 19] The mechanisms that cells use to read ultrafine nanoscale features are just beginning to be defined, and in this paper, we show that cells respond to interfacial surface energy. We show that cells respond to amazingly fine surface features that are near the limit of detection and that may be defined as interfacial surface energy. We demonstrate differences in growth, behavior, extracellular matrix (ECM) protein expression and adsorption, and adhesion of MDCK epithelial cells on three different SiO_2 substrates: amorphous glass coverslips (GCS) and the native oxide layers grown on ⟨111⟩ and ⟨100⟩ wafers. In this study, we show that the MDCK epithelial cells respond to subtle differences in substrate organization that is a function of either its atomic or crystal organization. Although all three surface materials are almost structurally and compositionally similar, we observe dramatic differences in the mechanical properties of the cell, cell morphology, cell–cell adhesion, cell–substrate adhesion, actin organization, ECM protein expression, and ECM protein for the various substrates. In concert with the experimental results, by modeling of surface energies, we demonstrate that the robust responses of MDCK cells to differences in substrate organization may be manifested through cell adhesion-based mechanisms that "read" differences in surface energy, either directly in the substrate or indirectly through ECM protein adsorption or organization on the surface.

2 Experimental Section

Cell Culture. MDCK cells were cultured with DMEM/high glucose (Hyclone Cat no. SH30022.01). Cells were transferred using 1× Trypsin/EDTA (MP #1689149) and Cell Striper (Corning REF: 25-056-Cl); MDCK cells required both methods for efficient removal. For 25 cm^2 flasks, we used 1.5 mL of each for 25 min at 37 °C. For 75 cm^2, we used 3 mL of each for

25 min at 37 °C. Cells were diluted at 40× for each experiment and were passed between 65 and 75% confluence.

Surface Preparation. Three specific silicon substrates were used: glass coverslips (GCS; Fisher product number 12345), ⟨111⟩ crystalline silicon wafer (111-SiW; Ted Pella product number 12345), and ⟨100⟩ crystalline silicon wafer (100-SiW; Ted Pella product number 12345). Surfaces were cleaned together with a standard RCA-1 cleaning procedure. Briefly, surfaces were washed in acetone for 15 min at 70 °C, washed with methanol for 5 min at room temperature, and then washed in a 1:1:5 solution of 30% hydrogen peroxide, 30% ammonium hydroxide, and DI water for 15 min at 70 °C. Surfaces were subsequently cleaned with an oxygen plasma cleaner (South Bay Technologies PC2000 Plasma Cleaner) to remove any potential residues after the RCA-1 cleaning procedure.

Force Modulation Mode (FMM) Atomic Force Microscopy (AFM) Methods. An Agilent 5600LS AFM and PicoView v.1.14 (Kesight Technologies, N9480S) was used for AFM work. Silicon nitride AFM probes (SINI-30, TED PELLA, INC) were used for imaging. Images were taken in FMM at a set point between 2 and 4 nN. Once a set point was chosen for an experiment, it was used for all trials. Scan speeds were 55 um/s. For the *z*-modulation in FMM, drive percentage was set to 10%, and the frequency was 30 kHz. This varied between tips and was set every time before experiments were done. The spring constant of each tip was determined for each experiment using Thermal-K in PicoView. MDCK cells were imaged on surfaces, untreated, in DMEM complete media. To reduce tip contamination, tips were coated with methoxy-triethyleneoxy propyltrimethoxy silane (SIM6493.4, Gelest, Inc.). Tips were plasma cleaned for 30 min. They were then immersed in the silane for one day. After this time, we used acetone to rinse the tips three times.

Confocal Microscopy Imaging of MDCK Cells. MDCK cells were cultured as described above on GSC or on ⟨111⟩ or ⟨100⟩ wafers for four days and then fixed in 4% formaldehyde in 1× phosphate buffered saline (PBS, pH 7.4) for 20 min. Cells were then labeled with mouse primary monoclonal antibodies (1:500 dilution in 1× PBS, 1% BSA, 0.1% Triton): E-cadherin (rr1; Developmental Studies Hybridoma Bank),[20] type II collagen (II-II6B3; Developmental Studies Hybridoma Bank),[21] collagenase pro-enzyme (H18G8; Developmental Studies Hybridoma Bank),[22] fibronectine III-15 (13G3B7; Developmental Studies Hybridoma Bank),[23] and S-laminin (C4; Developmental Studies Hybridoma Bank)[24] and a goat anti-mouse secondary antibody (Jackson laboratories, 1:2000 dilution). Cells were also counter-labeled with Hoescht to detect the DNA/nucleus (Molecular Probes/Life Technologies) and Alexa488 phalloidin (Molecular Probes/Lifetechnologies) to detect filamentous actin. All images were collected using Zeiss Observer Z.01 spinning disc confocal with Axiovision software. All images were collected using the same exposure times and laser settings. Densitometry data was collected from individual frames using the Interactive Measurement application within Axiovision. In the case of analyzing the intracellular amounts of ECM localization in the basal portions of MDCK cells, we collected data from *z*-sections that represented the bottom 0.5 υm of the cell. Densitometry data were statistically analyzed using Microsoft Excel software, specifically the *t*-test function.

Protein Adsorption Assays. Two assays were used to measure protein adsorption to the substrates. To measure the amount of proteins on the surface, we performed a modified reverse

dot blot assay. Substrates were incubated in DMEM media containing FCS for 24 h; samples were fixed with 4% formaldehyde, probed with the antibodies described in the previous methods section, and then detected using a goat anti-mouse secondary antibody that was conjugated with horseradish peroxidase. We also visualized protein on our surfaces using AFM. AFM images were obtained using an Agilent 5600 LS AFM. Surfaces were imaged using SiN4 tips (Ted Pella SINI-30) with a labeled force constant of 0.2 N/m. Measurements of the spring constant using the thermal-K tool available in Pico View 1.14 (Agilent) software gave values of k within the expected range of 0.2 ± 0.07 N/m. Deflection sensitivities were measured to be 75 ± 20 nm/V for all experiments. Surfaces were imaged at 1 line/s at 2 nN with a 25 um^2 field of view. Proteins were imaged using tapping mode with a tip of spring constant 40 N/m (Ted Pella TAP300-G-10 #). Ten micrometer images were taken at 1 line/s. Images were then processed using Pico View v.1.4. Adsorption was measured by counting structures larger than 10 nm, which were expected as a minimum size of the proteins.

Cell Growth and Wash Assays. Cell growth on the wafers was determined by counting the number of cells per field of view using the confocal microscope. Cells were cultured on a SiO_2 substrate for one to four days; on days one and four, cell-containing surfaces were collected, fixed, and stained with Hoechst, and the number of cells per field of view (FOV) were counted under the Zeiss Observer Z.01 spinning disc confocal microscope using the 20× objective. The relative adhesive strength of MDCK cell adhesion to a substrate was tested by treating cells cultured on a test substrates (GCS, ⟨111⟩ or ⟨100⟩) for one day; the cells were gently rinsed to remove nonadhered cells, stained with Hoechst, and then immediately counted using the confocal microscope 20 fields of view per sample. The same cell containing surfaces were then washed rigorously with 300 μL of 1× PBS 3 times and then reimaged as before. Experiment was repeated 3 times, and the significance was tested using a t-test.

3 Results

3.1 GCS, ⟨111⟩, and ⟨100⟩ Surface Characterization. Prior to determining the growth behaviors of epithelial cells on three different forms of SiO_2 (amorphous GCS, ⟨111⟩, and ⟨100⟩), we characterized these surfaces. As expected, all surfaces have similar structure, as all are flat (Figure 1), although the ⟨100⟩ substrates exhibit the ultrafine scale difference in nanotopography on the order of 1.5 nm ΔZ when compared to GCS and ⟨111⟩ substrates. GCS and the ⟨111⟩ wafers share a similar morphology with both presenting a regular set of wave-like contours across the surface, while the ⟨100⟩ Si wafer is relatively featureless (Figure 1). The variation between the surface properties of these three materials is subtle and interesting. In addition, Raman spectrometry and energy-dispersive X-ray spectroscopy (EDX) were used to verify the composition of each surface and showed no compositional differences between ⟨111⟩ and ⟨100⟩ substrates (Figures S1–S3). An ellipsometer was further used to measure the thickness of the oxide layer for the ⟨111⟩ and ⟨100⟩ silicon wafers. The oxide layer of ⟨111⟩ silicon wafer was measured to be 9.7 ± 2.5 nm, and the ⟨100⟩ silicon wafer was measured to be 10.1 ± 2.1 nm.

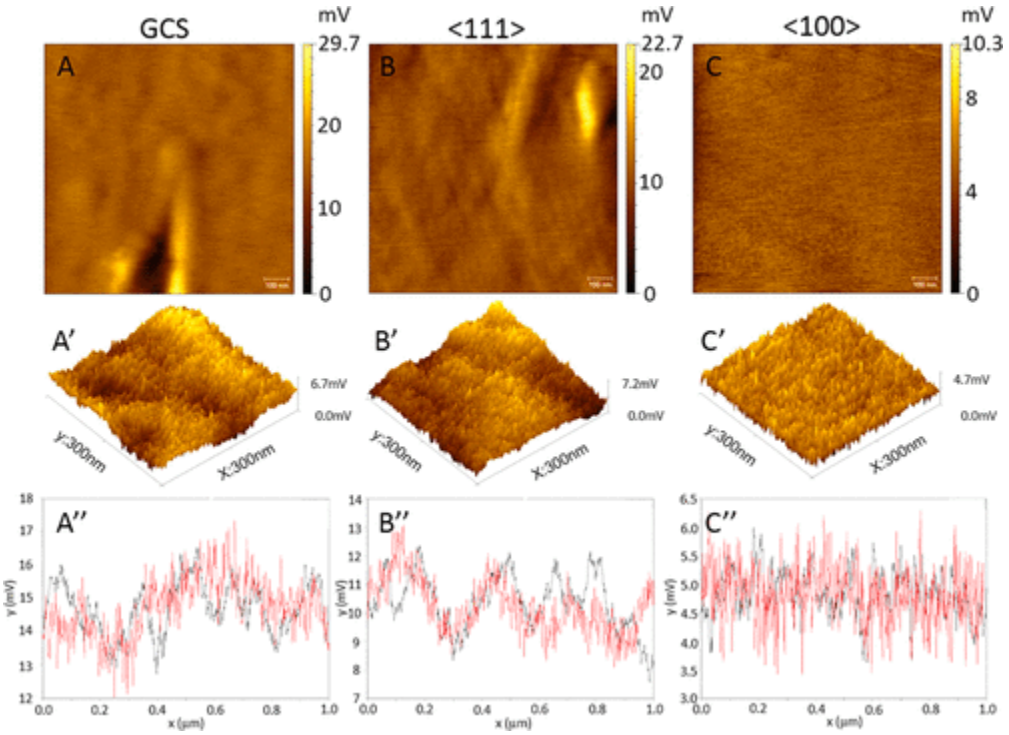

Figure 1. Atomic force micrographs of GCS, ⟨111⟩, and ⟨100⟩ substrates used in this study. Note that in A″–C″, black is *x* cross section, and red is *y* cross section.

3.2 Cellular Response to SiO_2 Substrates. To investigate the reaction that MDCK cells have to the three substrates (GCS, ⟨111⟩, and ⟨100⟩), we examined the growth of the cells, cell viability, and alteration to cell morphology. While we did not observe any change to the viability of MDCK cells grown on the surfaces, we observed significant differences in the morphology of MDCK epithelial cells on the three different forms of substrates. On average, both CGS and ⟨111⟩ substrates had similar number of cells per field of view after 4 days of culture (GCS, 75.2 ± 33; ⟨111⟩, 74.5 ± 22), while ⟨100⟩ has slightly fewer cells (58.8 ± 29). The slight reduction in the rate of growth was observed both on RCA-1 cleaned surfaces and plasma cleaned surfaces (see Methods), demonstrating that it was an inherent difference in the ⟨100⟩ surfaces themselves and not some residual effect of the substrate preparation (Figure S4).

However, MDCK cells expressed a strikingly different morphology when cultured on ⟨100⟩ SiO_2 substrates (Figure 2). MDCK cells cultured on GCS adopt a sheet squamous epithelium-like morphology with an average cell height of 2.4 μm (Table 1). This is demonstrated by short height of the cell in the *X*/*Z* projection (Figure $2A_{top}$) and the flat spread out cells in the sheet in the *X*/*Y* projection (Figure $2A_{bottom}$). MDCK cells cultured on ⟨111⟩ substrate have a flat morphology similar to that exhibited by GCS culture (Figure $2B_{top}$), and MDCK cells had an average cell height of 3.9 μm, although other morphology such as clustering (Table 1) was also observed. However, MDCK cells cultured on ⟨100⟩ wafers formed dense colonies of a taller cuboidal-like epithelium (Figure $2C_{top}$) with an average cell height of 13.9 μm (Table 1), roughly 4 times taller than MDCK cells grown on ⟨111⟩ wafers and GCS.

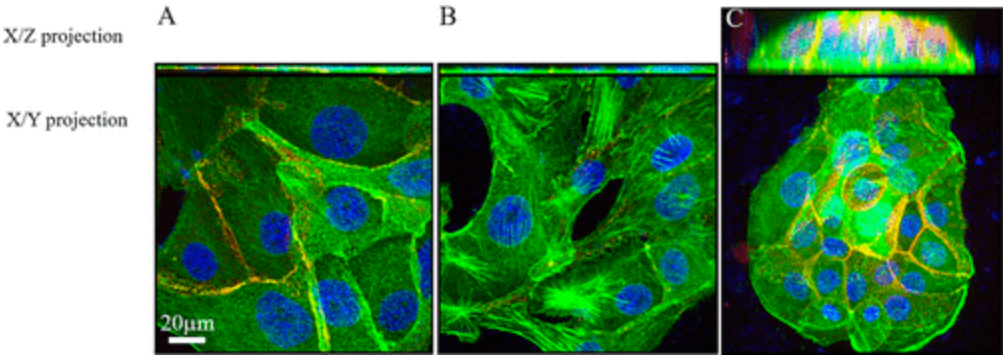

Figure 2. Confocal micrographs demonstrating the morphology of MDCK cells cultured on GCS (A) and Si wafers ⟨111⟩ (B) and ⟨100⟩ (C). The cells were triple labeled with Hoechst (blue), anticadherin (red), and Alexa488 phalloidin (green). Scale bar is 20 μm. The micrographs are 2D projects in the *X*–*Z* (top panel) and *X*–*Y* planes (bottom panel).

Table 1. Morphology of MDCK Cells on GCS, ⟨111⟩, and ⟨100⟩ Substrates

surface	morphology (%)	average cell height (μm)
GCS	sheet, 100%, $n = 44$	2.4 ± 0.5
⟨111⟩	sheet 72%, clustered 28%, $n = 43$	3.9 ± 1.8[a]
⟨100⟩	clustered 100%, $n = 45$	13.9 ± 7[b]

[a] Difference from GCS, highly significant P value < 0.001
[b] Difference from both GCS and ⟨111⟩, highly significant P value < 0.001

3.3 AFM Force Spectroscopy. To determine whether MDCK cells that were cultured on GCS, ⟨111⟩, or ⟨100⟩ substrates displayed altered mechanical properties, we examined the rigidity of live MDCK cells using AFM. AFM approaches have been used to examine adhesive forces in bacterial biofilm formation,[25, 26] changes in the yeast cell wall elasticity as a result of heat shock,[27] genetic cell wall studies in yeast,[28] and the mechanical aspects of apoptosis.[29-32] More recently, such AFM force spectrographic techniques have allowed the characterization of membrane blebbing in live motile cells,[33] adhesion forces in cardiac fibroblasts,[34] viral interactions with mammalian cells,[35] and the mechanical properties of epithelial cells during mitosis.[36] Our study is one of the first to examine the mechanical aspects of cell in a live epithelium. In this study, the deflection of an AFM probe was used to demonstrate the rigidity of the cell as it was imaged; simply put, the greater the deflection (the lighter the color) of the AFM probe's tip, the more rigid the sample (Figure 3A). Using this, we clearly show that the tall colonial MDCK cells that were grown on ⟨100⟩ substrates are nearly twice as rigid as those cultured on ⟨111⟩ substrates and more than twice as rigid as those cultured on GCS substrates (Figure 3B), which experimentally supports the significant differences in adhesive abilities of the three substrates. Herein, because surface energy is related to the work required to cleave a bulk sample, the rigidity difference of the cells by AFM force spectrography suggests that there is a significant difference in surface energies of the three substrates (which are calculated below).

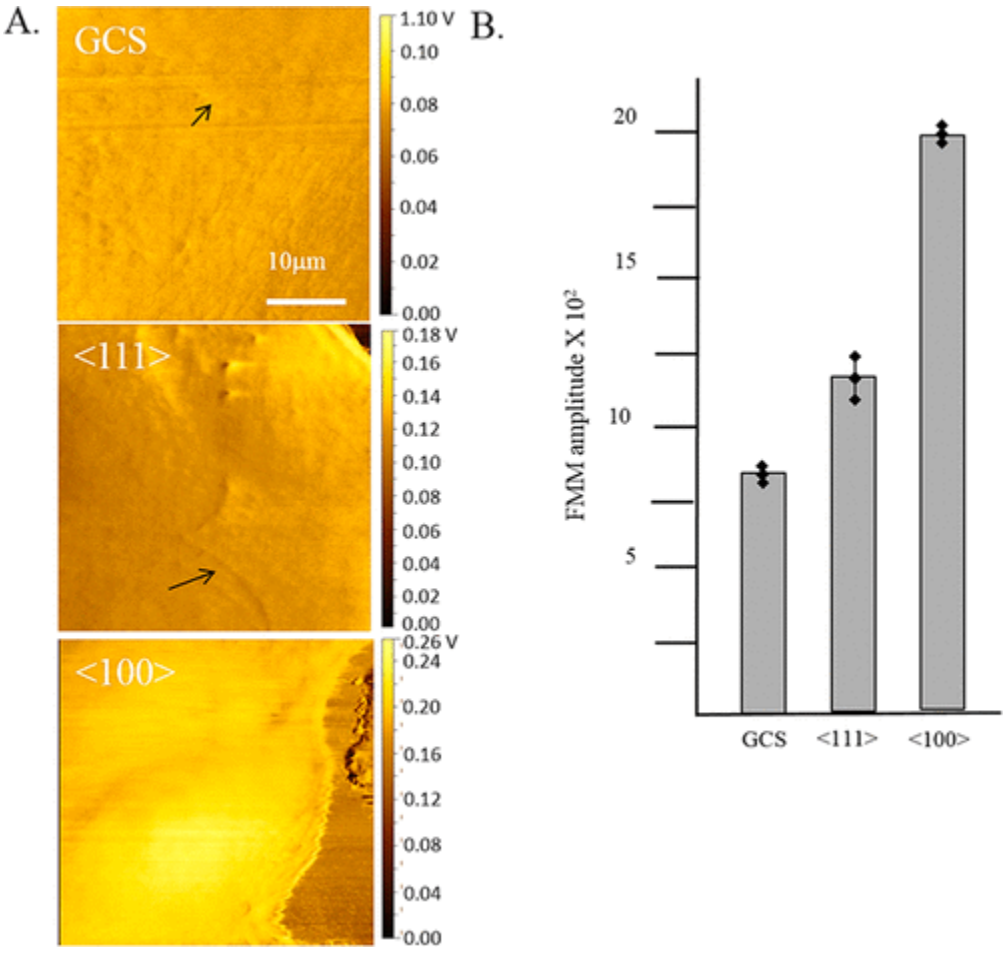

Figure 3. AFM Force amplitude images of MDCK cells cultured on GCS, ⟨111⟩, and ⟨100⟩ substrates. (A) AFM micrographs of MDCK cells cultured on GCS (top), ⟨111⟩ (middle), and ⟨100⟩ (bottom). The heat map ranges from light to dark with the lighter colors showing a greater deflection (i.e., greater rigidity of the cell). Not the ability to discern cell outlines (arrows in GCS and ⟨111⟩ micrographs). (B) Graphical description of the force amplitude images. The ⟨100⟩ surface has the highest average amplitude with significantly higher value when compared to ⟨111⟩ and GCS ($p < 0.001$).

3.4 Actin Organization. To determine whether these changes in cell–substrate adhesion and morphology reflect a change in the organization of the actin cytoskeleton, we examined the organization of filamentous actin in the cell cortex and in the basal regions of the cell that are in contact with the substrate. Adherent cells, both epithelial and fibroblastic, form characteristic bundles of actin called stress fibers that are indicative of adherence of the cell to the surface substrate though integrin-based complexes called integrin-based focal adhesions.[4, 37, 38] Cortical actin in MDCK cells grown on the ⟨100⟩ substrates appears denser (Figure 4C, thin arrow) than that grown on the other substrates (Figures 4A and B, arrow heads). By examining the first few confocal sections above the substrate, we observed basal actin location in the context of cell–substrate adhesion. Forty percent of the MDCK cells grown on GCS substrates have long and organized stress fibers (LOSF, i.e. fibers that extent along one axis in the cell); 12% of the cells having short and disorganized stress fibers (SDSF, i.e. fibers that had multiple directions in the cell), and 48% of the cells have no distinct stress fiber (NSF) (Table 2). In MDCK cells cultured

on ⟨111⟩ substrates, we observed an increased amount of SDSF and a slightly reduced amount of cells with longer stress fiber (Table 2). However, in MDCK cells grown on a ⟨100⟩ substrate, we observed a dramatic loss of all long and organized stress fibers and observed that most of the filamentous actin in the form of short and multioriented fibers (Figure 4C, arrow). This result strongly suggests that the mechanical interaction of the cell/⟨100⟩ is distinct and different from either the cell/GCS or cell/⟨111⟩ interaction. Furthermore, a cell-wash adhesion assay further demonstrates a reduced amount of cell–substrate adhesion between MDCK cells and ⟨100⟩ SiO_2 substrates (Figure 5).

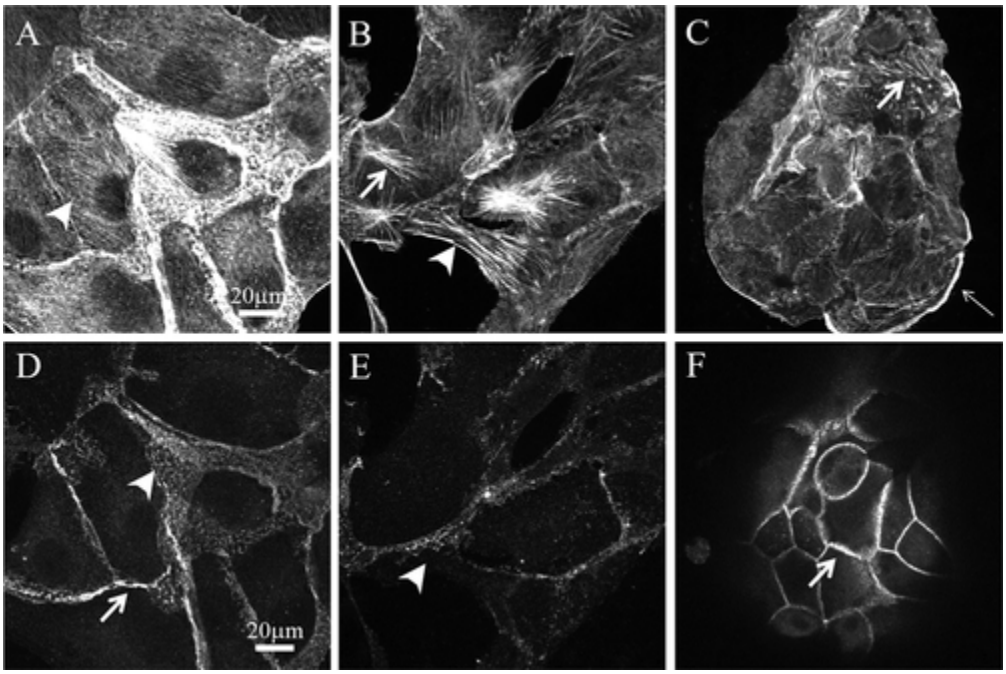

Figure 4. Basal actin and adherens junction organization in MDCK epithelial cells cultured on GCS (A, D), ⟨111⟩ (B, E), and ⟨100⟩ (C, F) substrates. (A–C) Basal filamentous actin organization in MDCK cells as shown by Alexa 488 phalloidin. (D–F) Adherens junction organization as shown by localization of cadherin.

Table 2. Basal Filamentous Actin and Adherens Junction (AJ) Organization in MDCK Cells Cultured on GCS, ⟨111⟩, and ⟨100⟩ Substrates

		basal actin organization (%)			AJ organization		cadherin levels	
surface	***n***	**LOSF**	**SDSF**	**NSF**	**% diffusive**	**% tight**	**average gray value**	**% change from GCS**
GCS	224	40	12	48	57 (*n* = 43)	43	5729 ± 1539	
⟨111⟩	85	34	28	38	64 (*n* = 44)	36	6157 ± 2828	103
⟨100⟩	133	0	59	41	9 (*n* = 45)	91	8997 ± 1772[a]	150[a]

[a] Difference from both GCS and ⟨111⟩, highly significant *P* value < 0.001

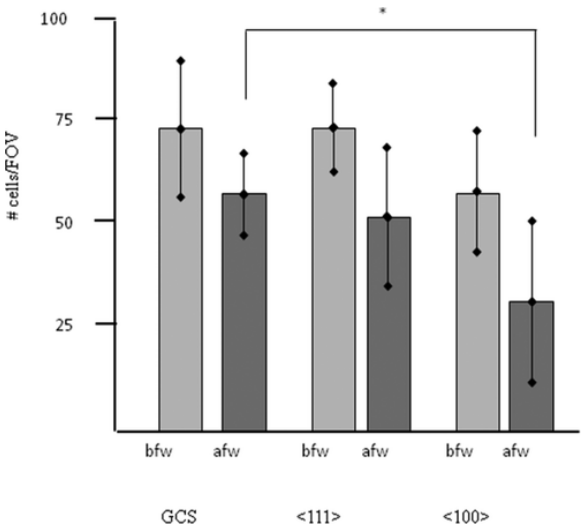

Figure 5. Cell wash assay on MDCK cells cultured on GCS, ⟨111⟩, and ⟨100⟩ substrates. MDCK cells were cultured on substrates for four days and subjected to a series of hydrodynamic wash cycles. Cells were then fixed and labeled with Hoechst, and the number of cells per field of view were counted before and after washing using confocal microscopy under the 20× objective. In each case, a similar fraction of cells were observed to be removed from both CGS and ⟨111⟩ substrate after the wash; however, MDCK cells cultured on ⟨100⟩ demonstrated significant reduction of cell/FOV after washing when compared to either GSC or ⟨111⟩ cells. $n = 20$, * represents $p < 0.05$.

Furthermore, epithelial cells have cell–cell adhesions that are mediated through supramolecular protein complexes called adherens junctions.[5, 10, 38, 39] Epithelial cells use these adherens junctions not only to maintain mechanical stability and control over the epithelium but also to direct and regulate intracellular signaling pathways.[10, 38] The basis of the adherens junctional complex is the homotypic interaction between two transmembrane cadherin proteins, which serves as the connection between neighboring cells within the epithelium; the intracellular cytoplasmic domain of the cadherin binds multiple adaptor molecules that bind the cortical actin cytoskeleton and function to maintain the mechanical and physical robustness of the linkage between cells.[10, 40] Changes in cadherin level or the type of cadherin molecules are indicative of both qualitative and quantitative properties of the adherens junction. For instance, increased cadherin within the adherens junction has shown to be directly associated with stronger cell–cell adhesion.[10, 39, 41] To determine whether culturing MDCK cells on ⟨100⟩ substrate results in an alteration to the cell–cell adherens junction, we examined the organization of the cell–cell contacts using an antibody directed against the cadherin-type expression in MDCK cells.[20] Significant quantitative and qualitative differences were observed in the organization of the adherens junctions in MDCK cells grown on ⟨100⟩; 91% of all the adherens junctions in MDCK cells grown on ⟨100⟩ have well-organized adherens junctions that extend the entire height of the cell (Figure 4F, arrow). In contrast, over half of the adherens junctions of cells grown on either GCS or ⟨111⟩ substrates are diffusive (Figures 4D and E, Table 2). Moreover, there is a significant increase in the amount of cadherin per unit area of adherens junction when compared to either cell grown on GCS or ⟨111⟩ substrate as determined by densitometry (Table 2).

3.5 Protein Adsorption. Because we observed significant changes in the manner that the MDCK cells interact with their substrate as well as with each other, we tested whether there was differential protein adsorption, specifically ECM protein adsorption to these different surfaces. The ECM is a complex material that is secreted from cells in the case of an epithelium; this matrix is often found on the basal lateral face.[42, 43] The ECM serves as a substrate for the growth and maintenance of epithelial cells as well as serving as a bulletin board for guidance cues and signals for migrating cells.[44] The ECM is composed of several major families of proteins, including collagens, laminins, and fibronectin. To determine whether ECM proteins interact with the different SiO_2 substrates, we evaluated the adsorption of purified ECM proteins (collagen II, s-laminin, and fibronectin) using a chemiluminescent surface analysis of ECM protein adsorption, an AFM-based technique, and fluorescently labeled proteins.

To examine the binding of ECM proteins to GCS, ⟨111⟩, and ⟨100⟩ substrates, we performed a modified immunological technique in which substrates were incubated with either cell culture medium with fetal bovine serum (FBS), probed with specific antibodies to ECM proteins, and then detected using an enzymatic chemiluminescent assay. These treated surfaces probed using antibodies directed against collagen II, s-laminin, or fibronectin. We observed differences in ECM protein adsorption to the different substrates and not all substrates interacting with the different proteins in a similar fashion. Also, we observed a decrease in collagen II, s-laminin, and fibronectin adsorption on ⟨100⟩ and ⟨111⟩ substrates when compared to GCS but the decrease on ⟨100⟩ is more remarkable (Figure 6).

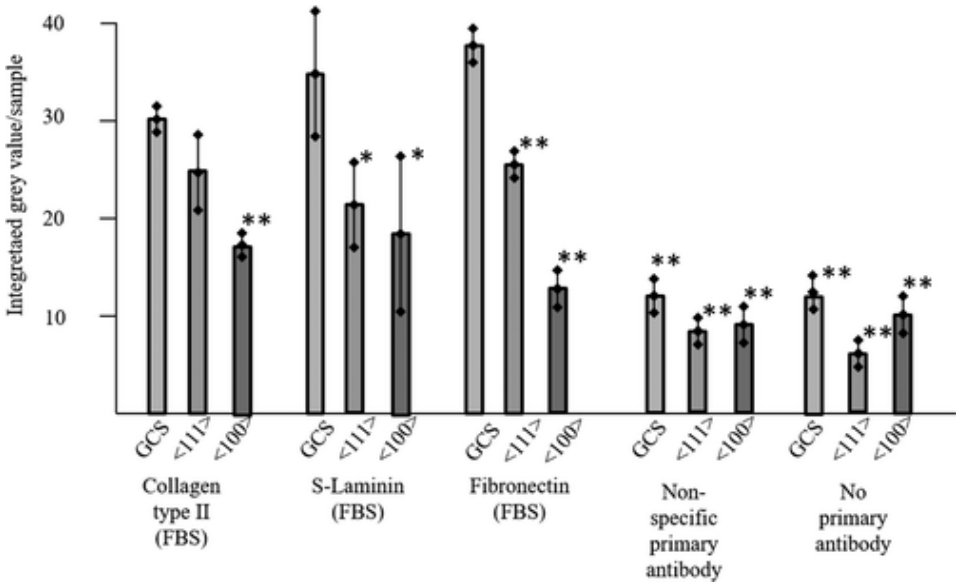

Figure 6. Chemiluminescent surface analysis of ECM protein adsorption on GCS, ⟨111⟩, and ⟨100⟩ substrates.

To complement the previous experiments, we also directly examined the binding of purified ECM proteins to GCS, ⟨111⟩, and ⟨100⟩ substrate using AFM. We treated each surface with purified collagen II (concentration) or laminin and then examined these surfaces using AFM contact mode to image protein deposition onto the surface (Figure 7). AFM analysis of the surfaces involved counting the number of features attached to the surface per unit area.[45] GCS substrates showed significantly more collagen II aggregate adsorption than the ⟨100⟩ substrate

and significantly more laminin than both ⟨111⟩ and ⟨100⟩ substrates. Further, there was a more remarkable decrease in collagen II and laminin adsorption on ⟨100⟩ substrates when compared to that on ⟨111⟩ substrates, which agrees with the experimental result above.

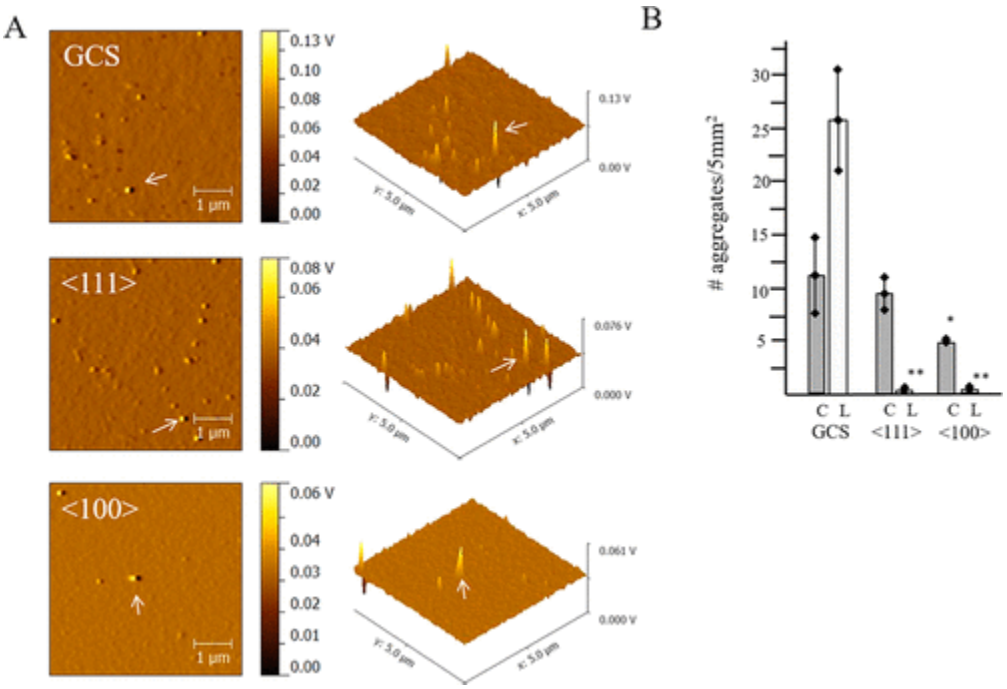

Figure 7. AFM analysis of ECM protein aggregating adsorption on GCS, ⟨111⟩, and ⟨100⟩ substrates. (A) AFM micrographs of collagen II aggregates on the substrates (GCS (top), ⟨111⟩ (middle), and ⟨100⟩ (bottom)). The first column is top-down images of the surfaces after adsorption, and the second columns are angle views of the aggregates on the surface. (B) Graph of the quantification of the number of aggregates (cologne II (C) and laminin (L)) per 5 μm^2 area on each surface. The number of protein aggregates as noted by the arrows in A were counted in ten fields, and their average with standard deviation is noted.

3.6 Alteration of ECM Protein Expression. On the basis of the protein adsorption results above, we need to clarify whether the MDCK cells may also respond to the subtle surface features through altered adhesion by remodeling their ECM as a response to the substrate because this type of response to changes in adhesive state and mechanical environment has been documented previously in a broad range of cell types.[22, 42, 44, 46-48] To determine the ECM protein expression, we examined the expression of several ECM proteins in these cells, including collagen II, s-laminin, fibronectin, and collagenase using confocal microscopy and immunofluorescence. In each case, we observed an increase in ECM protein expression in MDCK cells cultured on ⟨100⟩ substrates with the most dramatic increase in the expression in collagenase (Figure 8), indicating that high adhesive ability of ⟨100⟩ substrates (low ECM protein adsorption property) results in highly efficient ECM protein expression due to remodeling of ECM as a response to the ⟨100⟩ substrates. Note that the densitometry data were collected from the basal portion within the cell three confocal sections above the substrate, and data for each cell were defined and delineated by actin (see Figures 9A–C for details and Figure S5). Densitometry data for each cell were collected, statistically analyzed, and graphically depicted.

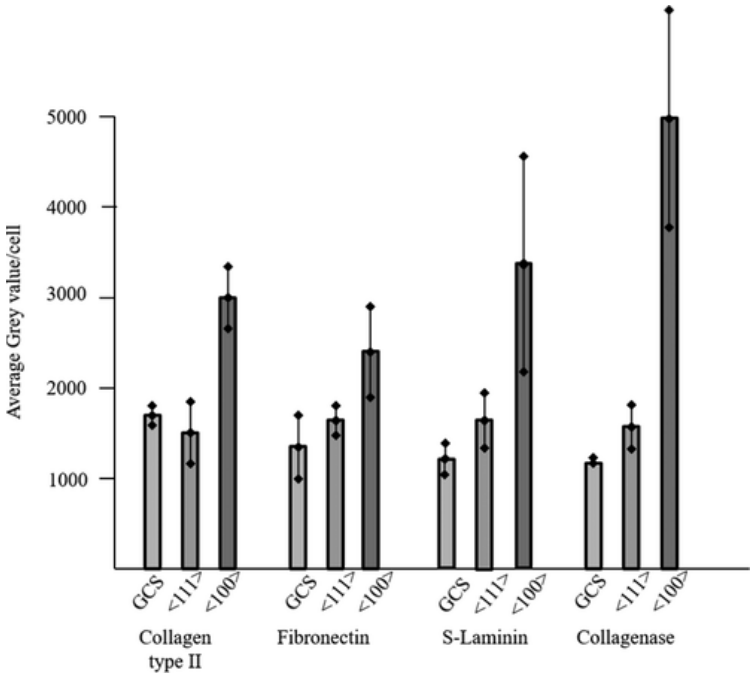

Figure 8. ECM protein expression levels in MDCK cells cultured on GCS, ⟨111⟩, and ⟨100⟩ substrates. Protein level expression whas determined using densitometry analysis of confocal images of cells probed using monoclonal antibodies for collagen II, fibronectin, s-laminin, and collagenase.

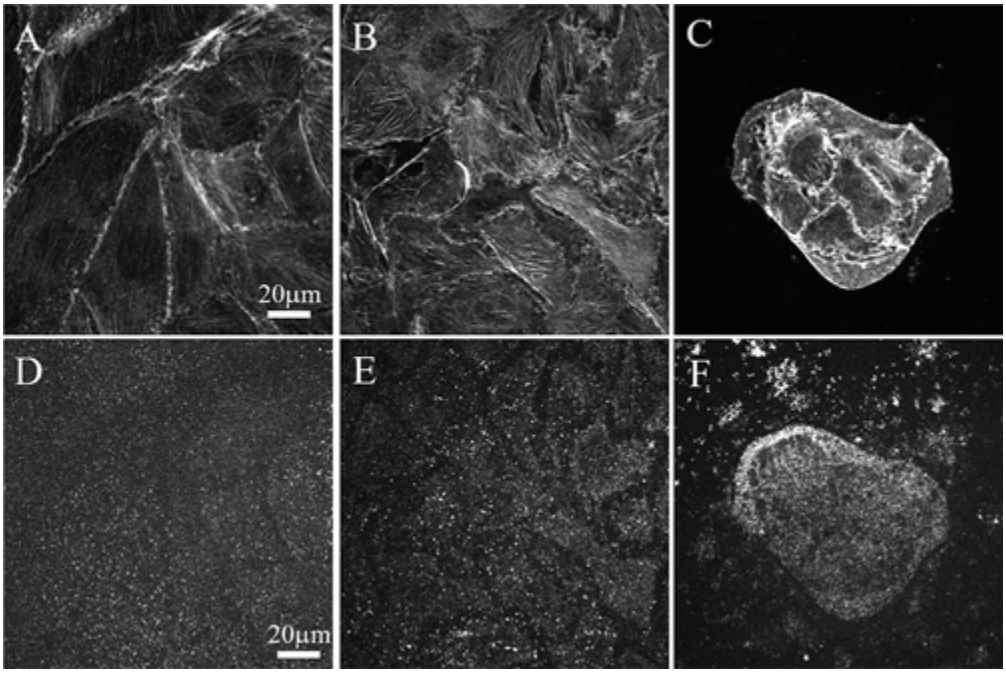

Figure 9. Fibronectin expression in MDCK epithelial cells cultured on GCS, ⟨111⟩, and ⟨100⟩ substrates. (A–C) Actin compared to (D–F) fibronectin organization. Long, well-organized stress fibers can be seen to correlate to consistent and even fibronectin organization.

3.7 Contact Angle and Estimation of Surface Energy for GCS, ⟨111⟩, and ⟨100⟩. Surface energy is an important parameter for surface characterization and searched as a fundamental means of defining the interfacial properties of a material. Contact angle measurements were taken to demonstrate variability in surface energy. Initial contact angle measurements on each surface using DI water had contact angles of 15.1 ± 1.0° for GCS, 8.4 ± 0.8° for ⟨111⟩, and 6.5 ± 1.6° for ⟨100⟩, demonstrating very hydrophilic surfaces. Contact angle measurements were used to determine surface energy with the flowing Young's equation:[49]

$$\gamma_s = \gamma_{sl} + \gamma_l \cos\theta \tag{1}$$

where γ_s is the surface energy of the solid, γ_{sl} is the surface energy of the solid covered with liquid, γ_l is the surface energy of the liquid, and θ is the contact angle. Undergoing a long development, the equation above reached its contemporary form as:[50]

$$\cos\theta = 2\sqrt{\frac{\gamma_s}{\gamma_l}}e^{-\beta(\gamma_l-\gamma_s)^2} - 1 \tag{2}$$

According to the equation above, in a figure of cosθ versus $1/(\gamma_l)^{1/2}$, the slope should be roughly equal to $2(\gamma_s)^{1/2}$, and the intercept should be −1. Based on this, Zisman reported that a plot of cosθ versus γ_l is often linear.[51] So, in terms of hydrophilic situation, smaller contact angle means larger surface free energy. According to our findings, although just minor differences, $\theta_{GCS} > \theta_{\langle 111\rangle} > \theta_{\langle 100\rangle}$; it still can be concluded that $\gamma_{GCS} < \gamma_{\langle 111\rangle} < \gamma_{\langle 100\rangle}$.

Regarding the surface energy difference of the SiO_2 layer between ⟨111⟩ and ⟨100⟩, qualitatively, different pure crystal reconstructions have different surface energies that depend on their orientations. Quantitatively, for the pure ⟨111⟩ and ⟨100⟩ (without SiO_2 layer), using a slab approximation model with periodic arrangements of slabs along the surface and with an assumption of centrosymmetric case, the surface energy could be calculated as the following equation:

$$\gamma^{n\times m} = \frac{E_{slab} - \Sigma_i N_i \mu_i}{2nmA} \tag{3}$$

where the same surface reconstruction $n \times m$ occurs on both sides of a material slab, E_{slab} is the total energy of a slab calculation with two identical surfaces, μ_i is the chemical potential of the surface constitute components allowing one to compare surfaces with different numbers of atoms in the two-dimensional surface unit cell, μ = −5.957 for Si, N_i is the number of the ith kind of atom per unit cell, and A is the unit cell area. In terms of the relaxed reconstruction with assumed averaged values for rest atoms,[52, 53] the averaged surface energies γ for pure ⟨111⟩ and ⟨100⟩ were estimated to be 1.63 and 1.94 J/m^2, respectively, attributed to the difference in the SiO_2 layer of ⟨111⟩ and ⟨100⟩.[54, 55]

Furthermore, to quantitatively determine the surface energy of different substrates, we used methyl iodide to measure the contact angles on each surface and obtained 46.7 ± 1.4° for GCS, 37.9 ± 0.7° for ⟨111⟩, and 35.2 ± 2.4° for ⟨100⟩ (Figure 9). To be able to calculate the surface

energy from the contact angle measurements, the interfacial tension (γ_{sl}) in eq 1 needs to be first determined. According to the Owens–Wendt–Rabel–Kaelble (OWRK) method,[56] the interfacial tension (γ_{sl}) is calculated by the following equation for the two measuring liquids because the estimation of surface energy of the substrate requires two liquids with known disperse and polar parts of the surface tension:

$$\gamma_{sl} = \gamma_s + \gamma_l - 2\left(\sqrt{\gamma_s^D \gamma_l^D} + \sqrt{\gamma_s^P \gamma_l^P}\right) \quad (4)$$

where γ^D and γ^P are the disperse part and polar part, respectively. Combining the results of contact angles of DI water and eq 1, the surface energy was estimated to be 56.12 ± 1.19 mJ/m^2 for GCS, 63.21 ± 1.07 mJ/m^2 for ⟨111⟩, and 65.29 ± 1.02 mJ/m^2 for ⟨100⟩, respectively (Figure 10). The order of surface energies for the three substrates strongly supports the experimental results mentioned above.

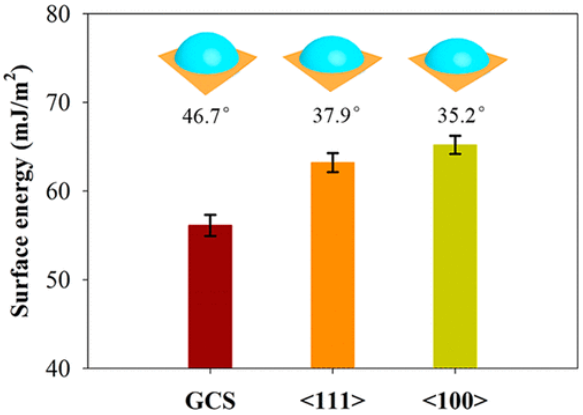

Figure 10. Surface energy calculated for GCS, ⟨111⟩, and ⟨100⟩ substrates tested by DI water and methyl iodide.

4 Discussion

Nanoscale materials change and control cellular adhesion, proliferation, and differentiation;[57, 58] however, what determines and defines these interactions is unclear. In addition to presenting limiting or functionalized surfaces that provide binding for a cell either directly to the surface or indirectly through the unusual display of specific ECM proteins,[45] nanoscale materials may also generate different mechanical landscapes for cells to engage.[6] Nanoscale features also alter surface chemistry when compared to bulk materials, which also have been shown to change cell behaviors.[59] In this study, we showed that MDCK epithelial cells read and respond to differences in the interfacial surface energy of a material, in this case SiO_2, although whether this is a direct effect of the cell interacting with the substrate or an indirect interaction through the display of the ECM proteins remains to be tested. However, SiO_2 surfaces did adsorb the least amount of ECM protein, which suggests that this feature may control the observed cellular responses. Although all three SiO_2 substrates used in this study have similar compositional and topographical features, we observed radically different responses in MDCK cell–substrate and cell–cell adhesion that manifest in distinct changes in the mechanical properties, protein expression, and cellular morphology. The most prominent of these morphological changes was

the transition of the MDCK cell epithelium from a flat squamous epithelium to a taller cuboidal epithelium. Similar increase to cadherin levels and epithelial cell morphology is observed in epithelial cells isolated germ layer from *Xenopus* embryos and are credited to alterations in the mechanical properties of the cell–cell interaction.[41] Changes in epithelial cell–cell adhesion have been shown to occur through changes in cell–substrate adhesion, which is controlled by interaction with ECM and other surface proteins.[60-65] We observe significant alteration to ECM protein adsorption on SiO_2 substrates derived from ⟨100⟩ Si wafers when compared to the other SiO_2 materials, and this may be the basis for the distinct cell behaviors that we observe. Protein interactions with silica materials have been shown to involve both polar and nonpolar interactions and are controlled by solvent conditions such as pH and the presence of soluble biomaterials such as hyaluronic acid as well as protein size and morphology.[66-69] Although the SiO_2 substrates have similar mechanical and compositional properties, they do have very subtle topographical differences that may contribute to some of the changes in cell behavior. Nevertheless, we showed that the surface energy of these materials is significantly different between the SiO_2 substrate derived from ⟨100⟩ and the other SiO_2 substrates. These data suggest that surface energy controls ECM protein adsorption, which then determines the behavior of the cell.

We have demonstrated that surface energy plays a significant role in the adsorption of ECM proteins, cell adhesion, and expression of ECM proteins. The adsorption interaction of ECM proteins with these different SiO_2 surfaces correlates with the hydrogen bond interactions of the SiO_2 surfaces with proteins. We applied a model to quantify the strength of the hydrogen bond interactions between the probe (−NH_2/–COOH) proteins, and the functional group (−OH) resulted from the presence of silanol groups (Si–OH) after the O_2 plasma treatment.[70, 71] These proteins are from one of three sources: (1) surface proteins of the MDCK epithelial cells, (2) proteins that have been secreted from the MDCK (i.e., ECM), or (3) proteins found in the serum of the media (or any combination of the three). This model assumes −OH for silanol groups and the following reaction for adhesion of a Si surface to probe hydrogen bonds:

$$-\mathrm{OH}\cdots\mathrm{H}-\mathrm{O}-\mathrm{H}+\mathrm{H}-\mathrm{O}-\mathrm{H}\cdots\mathrm{probe}\rightarrow-\mathrm{OH}\cdots\mathrm{probe}+2\mathrm{H_2O} \quad (5)$$

where – OH···H–O–H is the hydrated Si monolayer, H–O–H···probe is the hydrated probe, and −OH···probe is an adduct formed between Si monolayer and the probe. The net adhesion Gibbs free energy results are calculated such that $\Delta G(-\mathrm{OH}\cdots\mathrm{NH_2}-)_{\mathrm{net}}$ is −1680.66 J/mol and $\Delta G(-\mathrm{OH}\cdots\mathrm{COOH}-)_{\mathrm{net}}$ is −774.34 J/mol. It was concluded that the hydrogen bond adduct of NH_2–protein is easier to adhere than that of COOH–protein. In the case of the Si ⟨111⟩/oxide interface, the interaction between the dangling bonds and atoms in the oxide layer is weak because of the long distance between them. While in the case of the Si ⟨100⟩/oxide interface, the interaction is relatively strong because Si or oxygen atoms can be located close to the Si dangling bonds. Therefore, it is easier for Si ⟨111⟩/oxide interface to present Si–OH by the O_2 plasma treatment, which means that the density of Si ⟨111⟩–OH is higher than that of Si ⟨100⟩–OH.[71, 72] With the same unit ΔG (−OH···protein) as above, the total $-\Delta G$ value of $\mathrm{Si}\langle 111\rangle_{\mathrm{surface}}$ is higher than that of $\mathrm{Si}\langle 100\rangle_{\mathrm{surface}}$, indicating the adsorption ability of protein/⟨111⟩ is higher than that of protein/⟨100⟩. Similar study has demonstrated a similar phenomenon with the different crystal forms of TiO_2, and the hydroxyl ability affects a variety of cell behaviors including endothelial adhesion.[73] However, for the ECM protein expression, in each case we observed an increase in

ECM protein expression in MDCK cells cultured on ⟨100⟩ substrates, suggesting that high adhesive ability of ⟨100⟩ substrates causes highly efficient ECM protein expression due to remodeling of ECM as a response to the ⟨100⟩ substrates. This further suggests that the response of the MDCK cell to the substrate may be direct and through the changes mediated by differential cell–substrate adhesion directly affected the changes in the ECM organization or binding to the substrate. Eukaryotic cells display specific spatial requirements for the forming adhesive connections to both surface substrates and to other cells and use these connections to communicate, monitor, change, or maintain their differentiated state.[74]

Epithelial cells differ from mesenchymal cells in that they have and require cell–cell interactions for normal function and morphology.[64, 75] Epithelial cells form sheets of cells that are physically connected via adherens junctions, which link the cytoskeleton of one cell to another which adds an additional level of complexity in regards to mechanical sensing and signaling.[64, 65] Our results demonstrate that MDCK cells have a robust response to different SiO_2 substrates that correlates with the differential absorption of ECM protein. Differences in ECM protein absorption were not obviated by nanotopography and/or surface composition and correlate with differences in the surface energy of the different SiO_2 substrates. Although this work was performed using an epithelial tissue culture cell line, the characterization of radical differences in the cellular response to material with similar composition strongly suggests that other properties of a material other than composition and/or size must be considered when interpreting and controlling interactions of cells with a substrate.

5 Conclusions

While compositionally all three (GCS, ⟨111⟩, and ⟨100⟩) substrates are almost similar, compared to GCS and ⟨111⟩, the ⟨100⟩ substrate has the largest surface energy along with the highest adhesive ability, which results in dramatic differences in MDCK epithelial cell morphology, cell–cell adhesion, cell–substrate adhesion, actin organization, and ECM protein expression, although the ⟨100⟩ substrate has the lowest adsorption ability in ECM protein binding to the various substrates due to the hydrogen bond interactions. Our results demonstrate that MDCK cells have a robust response to differences in surface energies of the materials, suggesting that other properties of a material other than composition and topology should be considered when interpreting and controlling interactions of cells with a substrate, whether it is synthetic or natural.

Supporting Information

The Supporting Information is available at https://doi.org/10.1021/acsbiomaterials.7b00645.

References

1. Arnold, M.; Schwieder, M.; Blummel, J.; Cavalcanti-Adam, E. A.; Lopez-Garcia, M.; Kessler, H.; Geiger, B.; Spatz, J. P. Cell interactions with hierarchically structured nano-patterned adhesive surfaces Soft Matter **2009**, 5 (1) 72– 77 DOI: 10.1039/B815634D

2. Vignaud, T.; Galland, R.; Tseng, Q.; Blanchoin, L.; Colombelli, J.; Thery, M. Reprogramming cell shape with laser nano-patterning J. Cell Sci. **2012**, 125 (9) 2134– 2140 DOI: 10.1242/jcs.104901

3. Roca-Cusachs, P.; Iskratsch, T.; Sheetz, M. P. Finding the weakest link: exploring integrin-mediated mechanical molecular pathways J. Cell Sci. **2012**, 125 (13) 3025– 3038 DOI: 10.1242/jcs.095794

4. Yu, C. H.; Law, J. B.; Suryana, M.; Low, H. Y.; Sheetz, M. P. Early integrin binding to Arg-Gly-Asp peptide activates actin polymerization and contractile movement that stimulates outward translocation Proc. Natl. Acad. Sci. U. S. A. **2011**, 108 (51) 20585– 90 DOI: 10.1073/pnas.1109485108

5. Bhatt, T.; Rizvi, A.; Batta, S. P.; Kataria, S.; Jamora, C. Signaling and mechanical roles of E-cadherin Cell Commun. Adhes. **2013**, 20 (6) 189– 99 DOI: 10.3109/15419061.2013.854778

6. Darling, E. M.; Wilusz, R. E.; Bolognesi, M. P.; Zauscher, S.; Guilak, F. Spatial mapping of the biomechanical properties of the pericellular matrix of articular cartilage measured in situ via atomic force microscopy Biophys. J. **2010**, 98 (12) 2848– 56 DOI: 10.1016/j.bpj.2010.03.037

7. Morita, Y.; Kawase, N.; Ju, Y.; Yamauchi, T. Mesenchymal stem cell-induced 3D displacement field of cell-adhesion matrices with differing elasticities Journal of the mechanical behavior of biomedical materials **2016**, 60, 394– 400 DOI: 10.1016/j.jmbbm.2016.02.025

8. Chowdhury, F.; Na, S.; Li, D.; Poh, Y. C.; Tanaka, T. S.; Wang, F.; Wang, N. Material properties of the cell dictate stress-induced spreading and differentiation in embryonic stemcells Nat. Mater. **2010**, 9 (1) 82– 88 DOI: 10.1038/nmat2563

9. Engler, A. J.; Sen, S.; Sweeney, H. L.; Discher, D. E. Matrix Elasticity Directs Stem Cell Lineage Specification Cell **2006**, 126 (4) 677– 689 DOI: 10.1016/j.cell.2006.06.044

10. Ladoux, B.; Nelson, W. J.; Yan, J.; Mege, R. M. The mechanotransduction machinery at work at adherens junctions Integrative biology: quantitative biosciences from nano to macro **2015**, 7, 1109 DOI: 10.1039/C5IB00070J

11. Iannone, M.; Ventre, M.; Formisano, L.; Casalino, L.; Patriarca, E. J.; Netti, P. A. Nanoengineered surfaces for focal adhesion guidance trigger mesenchymal stem cell self-organization and tenogenesis Nano Lett. **2015**, 15 (3) 1517– 25 DOI: 10.1021/nl503737k

12. Moroni, L.; Licht, R.; de Boer, J.; de Wijn, J. R.; van Blitterswijk, C. A. Fiber diameter and texture of electrospun PEOT/PBT scaffolds influence human mesenchymal stem cell proliferation and morphology, and the release of incorporated compounds Biomaterials **2006**, 27 (28) 4911– 4922 DOI: 10.1016/j.biomaterials.2006.05.027

13. Gasiorowski, J. Z.; Murphy, C. J.; Nealey, P. F. Biophysical cues and cell behavior: The big impact of little things Annu. Rev. Biomed. Eng. **2013**, 15, 155– 176 DOI: 10.1146/annurev-bioeng-071811-150021

14. Kim, M. S.; Kim, A. Y.; Jang, K. J.; Kim, J. H.; Kim, J. B.; Suh, K. Y. Effect of nanogroove geometry on adipogenic differentiation Nanotechnology **2011**, 22 (49) 494017 DOI: 10.1088/0957-4484/22/49/494017

15. Jin, C. Y.; Zhu, B. S.; Wang, X. F.; Lu, Q. H.; Chen, W. T.; Zhou, X. J. Nanoscale surface topography enhances cell adhesion and gene expression of madine darby canine kidney cells J. Mater. Sci.: Mater. Med. **2008**, 19 (5) 2215– 2222 DOI: 10.1007/s10856-007-3323-z

16. Bhardwaj, G.; Webster, T. J. Increased NIH 3T3 fibroblast functions on cell culture dishes which mimic the nanometer fibers of natural tissues Int. J. Nanomed. **2015**, 10, 5293– 5299 DOI: 10.2147/IJN.S83007

17. Kam, K. R.; Walsh, L. A.; Bock, S. M.; Ollerenshaw, J. D.; Ross, R. F.; Desai, T. A. The effect of nanotopography on modulating protein adsorption and the fibrotic response Tissue Eng., Part A **2014**, 20 (1–2) 130– 138 DOI: 10.1089/ten.tea.2012.0772

18. Rebollar, E.; Frischauf, I.; Olbrich, M.; Peterbauer, T.; Hering, S.; Preiner, J.; Hinterdorfer, P.; Romanin, C.; Heitz, J. Proliferation of aligned mammalian cells on laser-nanostructured polystyrene Biomaterials **2008**, 29 (12) 1796– 1806 DOI: 10.1016/j.biomaterials.2007.12.039

19. Yu, J.; Huang, J.; Jansen, J. A.; Xiong, C.; Walboomers, X. F. Mechanochemical mechanism of integrin clustering modulated by nanoscale ligand spacing and rigidity of extracellular substrates Journal of the mechanical behavior of biomedical materials **2017**, 72, 29– 37 DOI: 10.1016/j.jmbbm.2017.04.018

20. Gumbiner, B.; Simons, K. A functional assay for proteins involved in establishing an epithelial occluding barrier: identification of a uvomorulin-like polypeptide J. Cell Biol. **1986**, 102 (2) 457– 468 DOI: 10.1083/jcb.102.2.457

21. Linsenmayer, T. F.; Hendrix, M. J. Monoclonal antibodies to connective tissue macromolecules: type II collagen Biochem. Biophys. Res. Commun. **1980**, 92 (2) 440– 6 DOI: 10.1016/0006-291×(80)90352-6

22. Werb, Z.; Tremble, P. M.; Behrendtsen, O.; Crowley, E.; Damsky, C. H. Signal transduction through the fibronectin receptor induces collagenase and stromelysin gene expression J. Cell Biol. **1989**, 109 (2) 877– 889 DOI: 10.1083/jcb.109.2.877

23. Burton-Wurster, N.; Lust, G. Molecular and immunologic differences in canine fibronectins from articular cartilage and plasma Arch. Biochem. Biophys. **1989**, 269 (1) 32– 45 DOI: 10.1016/0003-9861(89)90084-2

24. Hunter, D. D.; Shah, V.; Merlie, J. P.; Sanes, J. R. A laminin-like adhesive protein concentrated in the synaptic cleft of the neuromuscular junction Nature **1989**, 338 (6212) 229– 34 DOI: 10.1038/338229a0

25. Simoes, M.; Simoes, L. C.; Vieira, M. J. A review of current and emergent biofilm control strategies Lwt-Food Sci Technol **2010**, 43 (4) 573– 583 DOI: 10.1016/j.lwt.2009.12.008

26. Dufrene, Y. F.; Pelling, A. E. Force nanoscopy of cell mechanics and cell adhesion Nanoscale **2013**, 5 (10) 4094– 104 DOI: 10.1039/c3nr00340j

27. Pillet, F.; Lemonier, S.; Schiavone, M.; Formosa, C.; Martin-Yken, H.; Francois, J. M.; Dague, E. Uncovering by Atomic Force Microscopy of an original circular structure at the yeast cell surface in response to heat shock BMC Biol. **2014**, 12 (1) 6 DOI: 10.1186/1741-7007-12-6

28. Dague, E.; Bitar, R.; Ranchon, H.; Durand, F.; Yken, H. M.; Francois, J. M. An atomic force microscopy analysis of yeast mutants defective in cell wall architecture Yeast **2010**, 27 (8) 673– 684 DOI: 10.1002/yea.1801

29. Otto, K. Biophysical approaches to study the dynamic process of bacterial adhesion Res. Microbiol. **2008**, 159 (6) 415– 22 DOI: 10.1016/j.resmic.2008.04.007

30. Wang, D. C.; Chen, K. Y.; Tsai, C. H.; Chen, G. Y.; Chen, C. H. AFM membrane roughness as a probe to identify oxidative stress-induced cellular apoptosis Journal of biomechanics **2011**, 44 (16) 2790– 4 DOI: 10.1016/j.jbiomech.2011.08.021

31. Jin, H.; Zhao, H.; Liu, L.; Jiang, J.; Wang, X.; Ma, S.; Cai, J. Apoptosis induction of K562 cells by lymphocytes: An AFM study Scanning **2013**, 35 (1) 7– 11 DOI: 10.1002/sca.21028

32. Hu, M.; Wang, J.; Zhao, H.; Dong, S.; Cai, J. Nanostructure and nanomechanics analysis of lymphocyte using AFM: from resting, activated to apoptosis Journal of biomechanics **2009**, 42 (10) 1513– 9 DOI: 10.1016/j.jbiomech.2009.03.051

33. Gonnermann, C.; Huang, C.; Becker, S. F.; Stamov, D. R.; Wedlich, D.; Kashef, J.; Franz, C. M. Quantitating membrane bleb stiffness using AFM force spectroscopy and an optical sideview setup Integrative biology: quantitative biosciences from nano to macro **2015**, 7 (3) 356– 63 DOI: 10.1039/C4IB00282B

34. Sbaizero, O.; DelFavero, G.; Martinelli, V.; Long, C. S.; Mestroni, L. Analysis of long- and short-range contribution to adhesion work in cardiac fibroblasts: an atomic force microscopy study Mater. Sci. Eng., C **2015**, 49, 217– 24 DOI: 10.1016/j.msec.2014.12.083

35. Alsteens, D.; Newton, R.; Schubert, R.; Martinez-Martin, D.; Delguste, M.; Roska, B.; Müller, D. J. Nanomechanical mapping of first binding steps of a virus to animal cells Nat. Nanotechnol. **2016**, 12 (2) 177– 183 DOI: 10.1038/nnano.2016.228

36. Sorce, B.; Escobedo, C.; Toyoda, Y.; Stewart, M. P.; Cattin, C. J.; Newton, R.; Banerjee, I.; Stettler, A.; Roska, B.; Eaton, S.; Hyman, A. A.; Hierlemann, A.; Müller, D. J. Mitotic cells contract actomyosin cortex and generate pressure to round against or escape epithelial confinement Nat. Commun. **2015**, 6, 8872 DOI: 10.1038/ncomms9872

37. Sharma, S.; Grintsevich, E. E.; Phillips, M. L.; Reisler, E.; Gimzewski, J. K. Atomic force microscopy reveals drebrin induced remodeling of f-actin with subnanometer resolution Nano Lett. **2011**, 11 (2) 825– 7 DOI: 10.1021/nl104159v

38. Tolbert, C. E.; Burridge, K.; Campbell, S. L. Vinculin regulation of F-actin bundle formation: What does it mean for the cell? Cell Adh Migr **2013**, 7 (2) 219 DOI: 10.4161/cam.23184

39. Kim, Y. J.; Sauer, C.; Testa, K.; Wahl, J. K.; Svoboda, R. A.; Johnson, K. R.; Wheelock, M. J.; Knudsen, K. A. Modulating the strength of cadherin adhesion: evidence for a novel adhesion complex J. Cell Sci. **2005**, 118 (17) 3883– 94 DOI: 10.1242/jcs.02508

40. Caberlotto, E.; Michel, V.; de Monvel, J. B.; Petit, C. Coupling of the mechanotransduction machinery and F-actin polymerization in the cochlear hair bundles Bioarchitecture **2011**, 1 (4) 169– 174 DOI: 10.4161/bioa.1.4.17532

41. Ninomiya, H.; David, R.; Damm, E. W.; Fagotto, F.; Niessen, C. M.; Winklbauer, R. Cadherin-dependent differential cell adhesion in Xenopus causes cell sorting in vitro but not in the embryo J. Cell Sci. **2012**, 125 (8) 1877– 1883 DOI: 10.1242/jcs.095315

42. Kim, M. C.; Kim, C.; Wood, L.; Neal, D.; Kamm, R. D.; Asada, H. H. Integrating focal adhesion dynamics, cytoskeleton remodeling, and actin motor activity for predicting cell migration on 3D curved surfaces of the extracellular matrix Integrative Biology **2012**, 4 (11) 1386– 1397 DOI: 10.1039/c2ib20159c

43. Trache, A.; Trzeciakowski, J. P.; Meininger, G. A. Mg2+ modulates integrin-extracellular matrix interaction in vascular smooth muscle cells studied by atomic force microscopy J. Mol. Recognit. **2009**, 23 (3) 316– 321 DOI: 10.1002/jmr.985

44. Manzano, S.; Moreno-Loshuertos, R.; Doblare, M.; Ochoa, I.; Hamdy Doweidar, M. Structural biology response of a collagen hydrogel synthetic extracellular matrix with embedded human fibroblast: computational and experimental analysis Med. Biol. Eng. Comput. **2015**, 53 (8) 721– 35 DOI: 10.1007/s11517-015-1277-8

45. Keller, T. F.; Reichert, J.; Thanh, T. P.; Adjiski, R.; Spiess, L.; Berzina-Cimdina, L.; Jandt, K. D.; Bossert, J. Facets of protein assembly on nanostructured titanium oxide surfaces Acta Biomater. **2013**, 9 (3) 5810– 5820 DOI: 10.1016/j.actbio.2012.10.045

46. Rivera-Chacon, D. M.; Alvarado-Velez, M.; Acevedo-Morantes, C. Y.; Singh, S. P.; Gultepe, E.; Nagesha, D.; Sridhar, S.; Ramirez-Vick, J. E. Fibronectin and vitronectin promote human

fetal osteoblast cell attachment and proliferation on nanoporous titanium surfaces J. Biomed. Nanotechnol. **2013**, 9 (6) 1092– 1097 DOI: 10.1166/jbn.2013.1601

47. Cornelissen, C. G.; Dietrich, M.; Gromann, K.; Frese, J.; Krueger, S.; Sachweh, J. S.; Jockenhoevel, S. Fibronectin coating of oxygenator membranes enhances endothelial cell attachment Biomedical engineering online **2013**, 12 (1) 7 DOI: 10.1186/1475-925X-12-7

48. Springer, N. L.; Fischbach, C. Biomaterials approaches to modeling macrophage-extracellular matrix interactions in the tumor microenvironment Curr. Opin. Biotechnol. **2016**, 40, 16– 23 DOI: 10.1016/j.copbio.2016.02.003

49. Gindl, M.; Sinn, G.; Gindl, W.; Reiterer, A.; Tschegg, S. A comparison of different methods to calculate the surface free energy of wood using contact angle measurements Colloids Surf., A **2001**, 181 (1–3) 279– 287 DOI: 10.1016/S0927-7757(00)00795-0

50. Kwok, D. Y.; Lam, C. N. C.; Li, A.; Zhu, K.; Wu, R.; Neumann, A. W. Low-rate dynamic contact angles on polystyrene and the determination of solid surface tensions Polym. Eng. Sci. **1998**, 38 (10) 1675– 1684 DOI: 10.1002/pen.10338

51. David, R.; Neumann, A. W. Contact Angle Patterns on Low-Energy Surfaces Adv. Colloid Interface Sci. **2014**, 206, 46– 56 DOI: 10.1016/j.cis.2013.03.005

52. Shete, G.; Puri, V.; Kumar, L.; Bansal, A. Solid State Characterization of Commercial Crystalline and Amorphous Atorvastatin Calcium Samples AAPS PharmSciTech **2010**, 11 (2) 598– 609 DOI: 10.1208/s12249-010-9419-7

53. Liu, Q.; Hoffmann, R. The Bare and Acetylene Chemisorbed Si(001) Surface, and the Mechanism of Acetylene Chemisorption J. Am. Chem. Soc. **1995**, 117 (14) 4082– 4092 DOI: 10.1021/ja00119a024

54. Stekolnikov, A. A.; Furthmüller, J.; Bechstedt, F. Absolute surface energies of group-IV semiconductors: Dependence on orientation and reconstruction Phys. Rev. B: Condens. Matter Mater. Phys. **2002**, 65 (11) 115318 DOI: 10.1103/PhysRevB.65.115318

55. Eaglesham, D. J.; White, A. E.; Feldman, L. C.; Moriya, N.; Jacobson, D. C. Equilibrium shape of Si Phys. Rev. Lett. **1993**, 70 (11) 1643– 1646 DOI: 10.1103/PhysRevLett.70.1643

56. Żenkiewicz, M. Methods for the calculation of surface free energy of solids Journal of Achievements in Materials and Manufacturing Engineering **2007**, 24 (1) 137– 145

57. Anselme, K.; Davidson, P.; Popa, A. M.; Giazzon, M.; Liley, M.; Ploux, L. The interaction of cells and bacteria with surfaces structured at the nanometre scale Acta Biomater. **2010**, 6 (10) 3824– 3846 DOI: 10.1016/j.actbio.2010.04.001

58. Lord, M. S.; Foss, M.; Besenbacher, F. Influence of nanoscale surface topography on protein adsorption and cellular response Nano Today **2010**, 5 (1) 66– 78 DOI: 10.1016/j.nantod.2010.01.001

59. Lu, J.; Khang, D.; Webster, T. J. (2011) Enhanced vascular endothelial cell function on nanostructured titanium surface features: The role of nano to submicron roughness; MRS Proceedings. 1136. DOI: DOI: 10.1557/PROC-1136-DD04-04 .

60. Andresen Eguiluz, R. C.; Kaylan, K. B.; Underhill, G. H.; Leckband, D. E. Substrate stiffness and VE-cadherin mechano-transduction coordinate to regulate endothelial monolayer integrity Biomaterials **2017**, 140, 45– 57 DOI: 10.1016/j.biomaterials.2017.06.010

61. Baronsky, T.; Ruhlandt, D.; Brückner, B. R.; Schäfer, J.; Karedla, N.; Isbaner, S.; Hähnel, D.; Gregor, I.; Enderlein, J.; Janshoff, A.; Chizhik, A. I. Cell-Substrate Dynamics of the Epithelial-to-Mesenchymal Transition Nano Lett. **2017**, 17 (5) 3320– 3326 DOI: 10.1021/acs.nanolett.7b01558

62. Yeung, T.; Georges, P. C.; Flanagan, L. A.; Marg, B.; Ortiz, M.; Funaki, M.; Zahir, N.; Ming, W.; Weaver, V.; Janmey, P. A. Effects of substrate stiffness on cell morphology, cytoskeletal structure, and adhesion Cell Motil. Cytoskeleton **2005**, 60 (1) 24– 34 DOI: 10.1002/cm.20041

63. Cai, D.; Chen, S. C.; Prasad, M.; He, L.; Wang, X.; Choesmel-Cadamuro, V.; Sawyer, J. K.; Danuser, G.; Montell, D. J. Mechanical feedback through E-cadherin promotes direction sensing during collective cell migration Cell **2014**, 157 (5) 1146– 1159 DOI: 10.1016/j.cell.2014.03.045

64. Hannezo, E.; Prost, J.; Joanny, J. F. Theory of epithelial sheet morphology in three dimensions Proc. Natl. Acad. Sci. U. S. A. **2014**, 111 (1) 27– 32 DOI: 10.1073/pnas.1312076111

65. Ravasio, A.; Le, A. P.; Saw, T. B.; Tarle, V.; Ong, H. T.; Bertocchi, C.; Mège, R. M.; Lim, C. T.; Gov, N. S.; Ladoux, B. Regulation of epithelial cell organization by tuning cell– substrate adhesion Integrative Biology (United Kingdom) **2015**, 7 (10) 1228– 1241 DOI: 10.1039/C5IB00196J

66. Trachta, M.; Bludský, O.; Rubeš, M. The interaction of proteins with silica surfaces. Part I: Ab initio modeling Comput. Theor. Chem. **2017**, 1117, 100– 107 DOI: 10.1016/j.comptc.2017.07.019

67. Kurtz-Chalot, A.; Villiers, C.; Pourchez, J.; Boudard, D.; Martini, M.; Marche, P. N.; Cottier, M.; Forest, V. Impact of silica nanoparticle surface chemistry on protein corona formation and consequential interactions with biological cells Mater. Sci. Eng., C **2017**, 75, 16– 24 DOI: 10.1016/j.msec.2017.02.028

68. Berts, I.; Fragneto, G.; Porcar, L.; Hellsing, M. S.; Rennie, A. R. Controlling adsorption of albumin with hyaluronan on silica surfaces and sulfonated latex particles J. Colloid Interface Sci. **2017**, 504, 315– 324 DOI: 10.1016/j.jcis.2017.05.037

69. Zerfass, C.; Braukmann, S.; Nietzsche, S.; Hobe, S.; Paulsen, H. High yield recombinant production of a self-assembling polycationic peptide for silica biomineralization Protein Expression Purif. **2015**, 108, 1– 8 DOI: 10.1016/j.pep.2014.12.012

70. Liu, H.; Yamamoto, H.; Wei, J.; Waldeck, D. H. Control of the electron transfer rate between cytochrome c and gold electrodes by the manipulation of the electrode's hydrogen bonding character Langmuir **2003**, 19 (6) 2378– 2387 DOI: 10.1021/la026378n

71. Cong, C.; Li, K.; Zhang, X. X.; Yu, T. Visualization of arrangements of carbon atoms in graphene layers by Raman mapping and atomic-resolution TEM Sci. Rep. **2013**, 3, 1 DOI: 10.1038/srep01195

72. Inglesfield, J.E. Surface electronic structure. Reports on Progress in Physics, 1982. 45 (3): p. 223− 284.

73. Li, X. C.; Chen, J. Y.; Xu, L.; Huang, N. The investigation of the hydroxyl activity ability on Ti-O film surface with different structure and its influence to biocompatibility Gongneng Cailiao/Journal of Functional Materials **2008**, 39 (8) 1359– 1362

74. Wang, H. J.; Cao, Y.; Sun, Y. Y.; Wang, K.; Cao, C.; Yang, L.; Zhang, Y. D.; Zheng, Z.; Li, D.; Wang, J. Y.; Han, Y. L. Is there an optimal topographical surface in nanoscale affecting protein adsorption and cell behaviors? J. Nanopart. Res. **2011**, 13 (9) 4201– 4210 DOI: 10.1007/s11051-011-0364-5

75. Chung, I. M.; Enemchukwu, N. O.; Khaja, S. D.; Murthy, N.; Mantalaris, A.; García, A. J. Bioadhesive hydrogel microenvironments to modulate epithelial morphogenesis Biomaterials **2008**, 29 (17) 2637– 2645 DOI: 10.1016/j.biomaterials.2008.03.008